EMI from Shielding Enclosures—FDTD Modeling and Measurements

Min Li
Electromagnetic Compatibility Laboratory
University of Missouri-Rolla
mili@ece.umr.edu

I. Introduction

The integrity of shielding enclosures for high-speed digital designs is compromised by slots and apertures for heat dissipation, CD-ROMs, I/O cable penetration, and plate-covered unused connector ports, among other possibilities. Radiation from slots and apertures in conducting enclosures excited by interior PCB level sources is of great concern in meeting FCC radiated EMI limits. At frequencies above the fundamental cavity-mode resonance, radiation from enclosure perforations can dominate radiation from I/O cables connecting the high-speed PCB to peripherals. An understanding of energy coupling mechanisms to and from the enclosure, as well as an experimentally verified modeling approach is essential in minimizing the EMI and susceptibility risk in a new design.

This summary details modeling of EMI coupling through slots and apertures at cavity mode resonances, as well as new resonances associated with the interaction between the cavity and slot, and resonances due to the slots and apertures. EMI from perforations in a shielding enclosure was studied experimentally and with finite-difference time-domain (FDTD) modeling. Among the significant results is that EMI at cavity mode resonances through non-resonant slots or apertures can be as significant as that from resonant slots and apertures. The EMI from closely-spaced multiple electrically short slots is proportional to the number of slots. Good agreement between the measurements and modeling shows that numerical modeling of enclosure designs can be a useful aid in understanding fundamental coupling physics and in developing EMI design guidelines for enclosures.

II. Problem Description

EMI from shielding enclosures was studied using a simple rectangular shielding enclosure, which accommodated straightforward identification of cavity modes. The geometry of this enclosure is shown in Figure 1. The enclosure was constructed of five pieces of *0.635-cm* thick aluminum, and one plate of *0.05-cm* thick aluminum for the face containing the slot or aperture. The cavity was constructed so that it could easily be disassembled and reassembled for repeatable measurements. The inside dimensions of

the enclosure were *22 cm* × *14 cm* × *30 cm*. One-inch copper tape with a conductive adhesive was used as an electromagnetic seal along the seams in the interior.

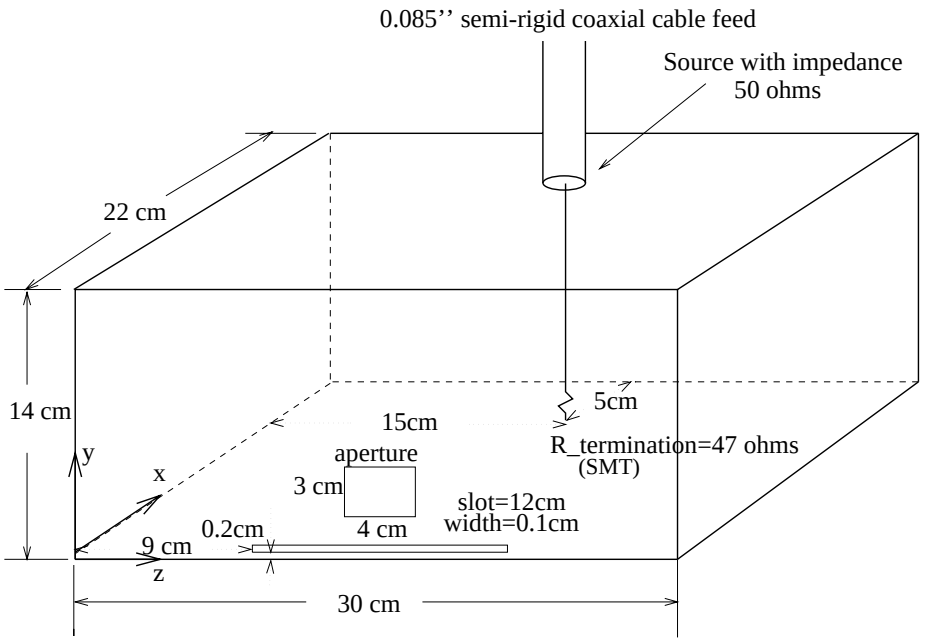

Figure 1. A rectangular test enclosure.

The cavity was fed with a *50Ω* coaxial cable probe through a type-N bulkhead connector, which was peripherally bonded to the cavity. The excitation, as shown in Figure 1, had the center conductor of the probe extended to span the width of the cavity with a *0.16-cm* diameter wire, and terminated on the opposite cavity wall with a 1206 package size surface-mount (SMT) nominal *47Ω* resistor soldered to a *1.5''* ×*1.5''* square of conductive adhesive copper tape. This source geometry was employed in order to introduce the loss necessary in the FDTD modeling. The type N bulkhead connector was located at *x=17 cm, y=14 cm, z=15 cm.*

The finite-difference time-domain (FDTD) method was used to model the test enclosure excited by a terminated feed probe. A cell size of *1.0 cm* × *0.5 cm* × *1.0 cm* was employed in the FDTD modeling. A finer discretization along the *y* direction was used in order to better model the spatial extent of the SMT load resistor. Aluminum plates were modeled with PEC surfaces by setting the tangential electric field to zero on the cavity walls. The feed probe was modeled by a simple voltage source *Vs* with *50-Ω* resistance incorporated into a single cell at the feed point. The magnetic fields circling the source were modeled in the same fashion as a thin wire to give the cross-section of the source with the specified physical dimensions [1]. The resistor was modeled as a lumped element using a subcellular algorithm [2]. The width of the SMT is approximately that of the feed wire diameter and the physical cross-section dimensions were modeled with the same diameter as that of the feed wire by modifying the magnetic field components circling the SMT in the same fashion as for the source. Thin slots were

modeled with the capacitive thin slot formalism (C-TSF) introduced by Gilbert and Holland [3], as applied to shielded enclosures [4].

The far-zone field was obtained by applying equivalence theory to the numerical FDTD modeling results. The FDTD method was used to calculate the electric and magnetic fields on a virtual surface completely surrounding the FDTD model of the enclosure. From the modeled values of the electric and magnetic fields on this surface, equivalent magnetic and electric surface current distributions were determined. The electric and magnetic vector potentials, in the frequency domain, are related to the electric and magnetic surface current distributions on a virtual surface *S'*, through [5]

$$\vec{A}(\vec{r},\omega) = \frac{\mu_0}{4\pi}\int_{s'} \vec{J}_s(\vec{r}',\omega)\frac{e^{-jk|\vec{r}-\vec{r}'|}}{|\vec{r}-\vec{r}'|}ds', \tag{1}$$

$$\vec{F}(\vec{r},\omega) = \frac{\varepsilon_0}{4\pi}\int_{s'} \vec{M}_s(\vec{r}',\omega)\frac{e^{-jk|\vec{r}-\vec{r}'|}}{|\vec{r}-\vec{r}'|}ds'. \tag{2}$$

The far-zone electric field components, $E_\theta(\vec{r},\omega)$ and $E_\phi(\vec{r},\omega)$ are then

$$E_\theta(\vec{r},\omega) = -j\omega[A_\theta(\vec{r},\omega) + \eta F_\phi(\vec{r}.\omega)], \tag{3}$$

$$E_\phi(\vec{r},\omega) = -j\omega[A_\phi(\vec{r},\omega) - \eta F_\theta(\vec{r}.\omega)]. \tag{4}$$

Equation (1) and (2) in the time domain are implemented in the FDTD modeling [6], and the far-zone electric field is obtained using an FFT from Equation (3) and (4).

The virtual surfaces were placed 6 cells away from the enclosure in the FDTD modeling. Perfectly-Matched-Layer (PML) absorbing boundary conditions were employed for the 3D FDTD modeling [7]. The PML absorbing layers were 8 cells away from the conducting planes without the slot, and 12 cells away from the conducting planes containing or near the slot.

S-parameters and radiated EMI measurements were also performed in a *3 m* anechoic chamber. Two-port S-parameters were measured with a Wiltron 37247A network analyzer. Port 1 was connected to the interior source in the enclosure under test, and Port 2 was connected to a receiving antenna. The network analyzer was placed outside the anechoic room to measure the reflection coefficient, $|S_{11}|$, and the transmission coefficient, $|S_{21}|$. The power delivered to the enclosure is related to the reflection coefficient as [8]

$$P = \frac{V_s^{\,2}}{8Z_0}(1-|S_{11}|^2), \tag{5}$$

where V_s is the source voltage, and Z_0 is the source impedance as well as the characteristic impedance of the coaxial cable. In this particular case the source voltage is scaled to *1 mV* for the purpose of comparing with the FDTD modeling, and the source impedance equals the characteristic impedance (*50* Ω)of the coaxial cable connected to Port 1 and and Port 2. The available power is then *2.5 nW*.

Far-zone electric field measurements were made with a separation of *3 m* between the enclosure and the receiving antenna. The far-zone electric field provides a quantitative measurement of the EMI level and is related to the S-parameters by [9]

$$E_{far} = AF \times |S_{21}| \times 0.5V_s \quad (6)$$

where *AF* is the antenna factor of the receiving antenna. The enclosure resonances and slot resonances are determined from the delivered power, and the far-zone electric field indicates EMI peaks. From the relation between delivered power and far-zone fields, the coupling of EMI from the shielding enclosure can be studied.

The electronics in a real product enclosure are usually too complicated to be directly modeled with any numerical method. From measurements on a computer server enclosure with electronics, the loading effect of electronics is known to be appreciable [10]. Lossy materials may be used in the enclosure to mimic the loading effect of the electronics for FDTD modeling purposes, and the effect of conductive lossy materials was also studied herein. Two layers of Milliken conductive *110-*Ω */*square lossy material were placed on the *x=22-cm* interior plane. The thickness for each layer was *0.4-cm*, and the conductivity of the lossy material used in the FDTD modeling was $\sigma = \frac{1}{R\,d} = 0.227 S/cm$. The lossy material was simply modeled by a one-cell layer of conducting material with conductivity $\sigma = 0.227 S/cm$. For the electric field components inside the conducting layer, the conductivity $\sigma = 0.227 S/cm$ was employed, while the conductivity $\sigma = \frac{0.227}{2} S/cm$ was employed for the components on the interface of the conducting layer and free space.

III. Results and Discussion

Measurements and FDTD modeling were conducted on the rectangular test enclosure with a *12-cm* long and *0.1-cm* wide thin slot as shown in Figure 1. The results of delivered power and far-zone electric field (at *3 m*) are shown in Figure 2. The frequency range studied was from *0.7 GHz* to *1.6 GHz*, which included several cavity modes, as well as the slot half-wavelength resonance. The agreement between the measurements and modeling is good in both cases. The cavity mode resonances, and the resonances due to the slot were distinguished by observing the delivered power measurements as the slot length was varied. With the reduction of slot length, the cavity mode resonance frequencies were almost unchanged, and the resonances due to the slot disappeared from this frequency range.

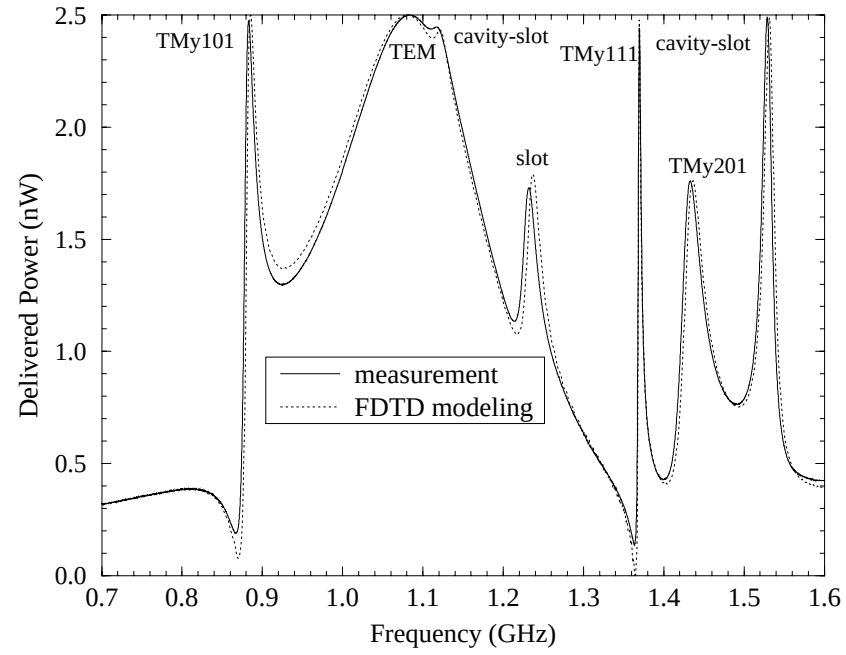

(a)

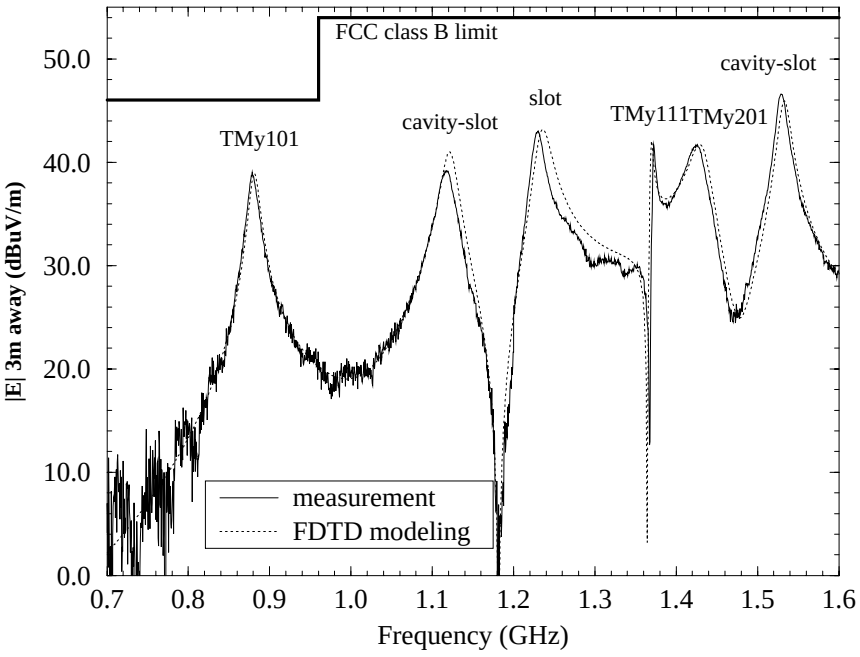

(b)

Figure 2. Measured and modeled results for the test enclosure with a *1 mV* source for (a) delivered power, and (b) electric field at *3 m*.

Radiation from an aperture was also considered. In this case a rectangular aperture, measuring *3 cm* × *4 cm* and centered at *y=5.5 cm, z=15 cm* was cut into the front wall of the cavity, as shown in Figure 1. In applying the FDTD modeling for this case, the result

of electric field at *3 m* using the 1.*0-cm* × *0.5-cm* × *1.0-cm* cell size (*24* cells in the aperture) was generally *5 dB* below the measured result. Then the computational cell size was reduced to *0.5 cm* × *0.5 cm* × *0.5 cm* in order to increase the number of FDTD cells modeling the aperture to *48* cells. An improvement of *3 dB* was obtained. The measured and FDTD modeling results of both the delivered power and the electric field at *3 m* are shown in Figure 3. The change of the cell size had no significant effect on the FDTD modeling of the delivered power, since the power radiated from the aperture was only a small fraction of the total delivered power. The three large, broad peaks in the far zone electric field intensity correspond to cavity-mode resonances at *0.885 GHz, 1.4 GHz*, and *1.5 GHz.* Narrow bandwidth peaks occur at *1.18 GHz* and *1.36 GHz* and are associated with the presence of the aperture. Nevertheless, the highest frequency (*1.6 GHz)* in this measurement is well below the first aperture resonance.

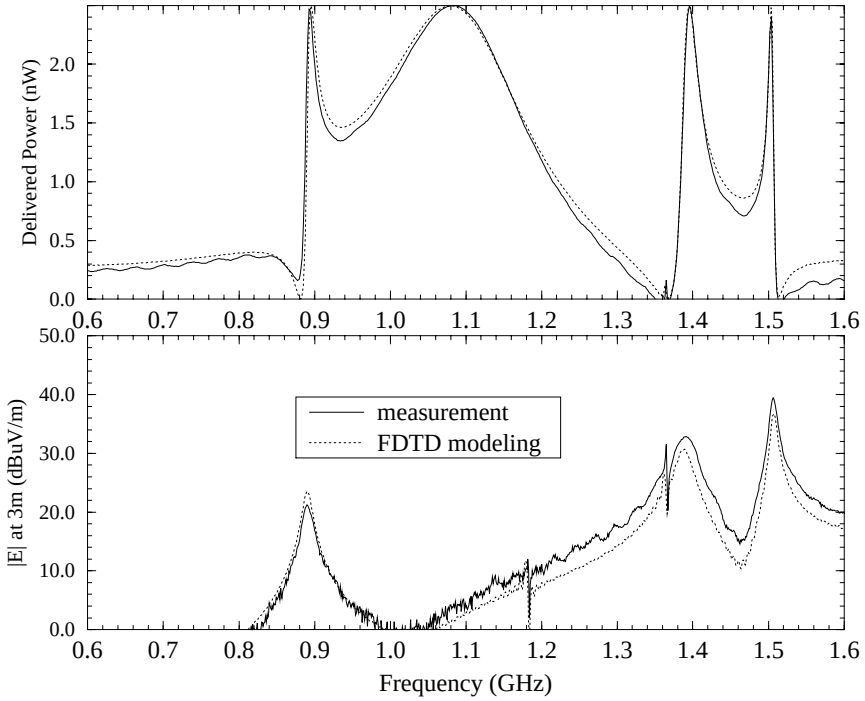

Figure 3. The measured and modeled delivered power and electric field strength *3 m* away through a *3-cm* × *4-cm* aperture in test enclosure.

Multiple slots were also investigated to study EMI at cavity mode resonances. Two parallel *5 cm* slots on the same face *x=0* were employed with a distance of *0.9-cm* edge-to-edge spacing. The left end of the slots was *9-cm* from the *x=0,z=0* edge. Measurement and FDTD modeling results, consisting of the delivered power and the electric field at *3 m*, are shown in Figure 4. The cavity-mode resonances in this frequency range can be identified as *TMy101*, *TMy111*, and *TMy201* at *0.885 GHz*, *1.4 GHz*, and *1.5 GHz*, respectively. The electric field plots show that these cavity resonances are associated with significant peaks in the radiated EMI level. There is also a peak in the electric field at *3 m* at a frequency of approximately *1.36 GHz*. This peak represents a cavity-slot resonance and is unlikely to be associated with high levels of EMI when the enclosure is

excited by active digital electronics since this peak has a very narrow bandwidth. Further, incorporating the effects of loss will appreciably damp this high-Q resonance. In comparing the radiated electric field from a single *5-cm* slot with that from a pair of closely spaced *5-cm* slots located in the same wall of the cavity, the double slot configurations were approximately *6 dB* higher, i.e., the EMI is varying as N the number of slots [6].

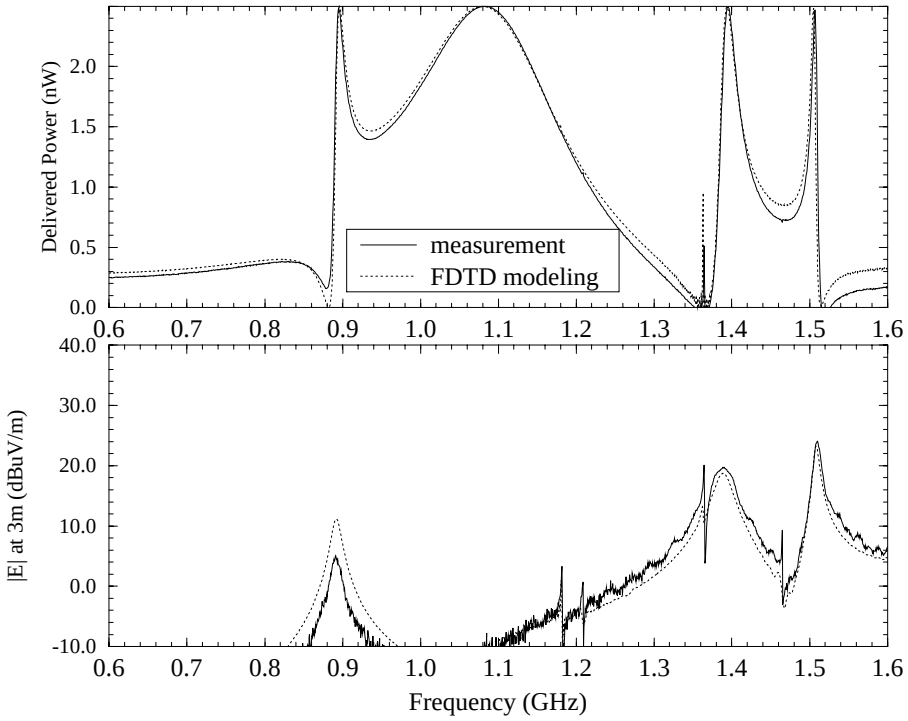

Figure 4. Measured and modeled electric field at 3 m for two parallel *5-cm* long slots.

The measured and modeled delivered power and electric field strength at *3 m* with the lossy material on the interior face *x=22 cm* are shown in Figure 5. The agreement between the measurements and FDTD modeling is generally good. The effect of the lossy material in decreasing the Qs of resonances is evident in the delivered power, and reflected in the reduced radiation in the *3 m* electric field, e.g., the *TMy101* mode at *0.89 GHz*, the *TMy111* mode at *1.36 GHz*, the *TMy201* mode at *1.44 GHz*, and the resonance at *1.53 GHz*. However, a resonance and a corresponding increase in radiation were observed at *1.20 GHz*, where the two resonances due to the slot at *1.10 GHz* and *1.24 GHz* for the situation without the lossy material may have shifted and broadened to produce a resonance at *1.20 GHz*. Overall, a lossy material can be easily incorporated in the FDTD modeling, and may be used to mimic the electronics in the initial shielding enclosure design stage. For example, a conducting plane with a lossy dielectric on it can be used to approximate a PCB (that has entire power or ground planes) with electronics for FDTD modeling of enclosure designs.

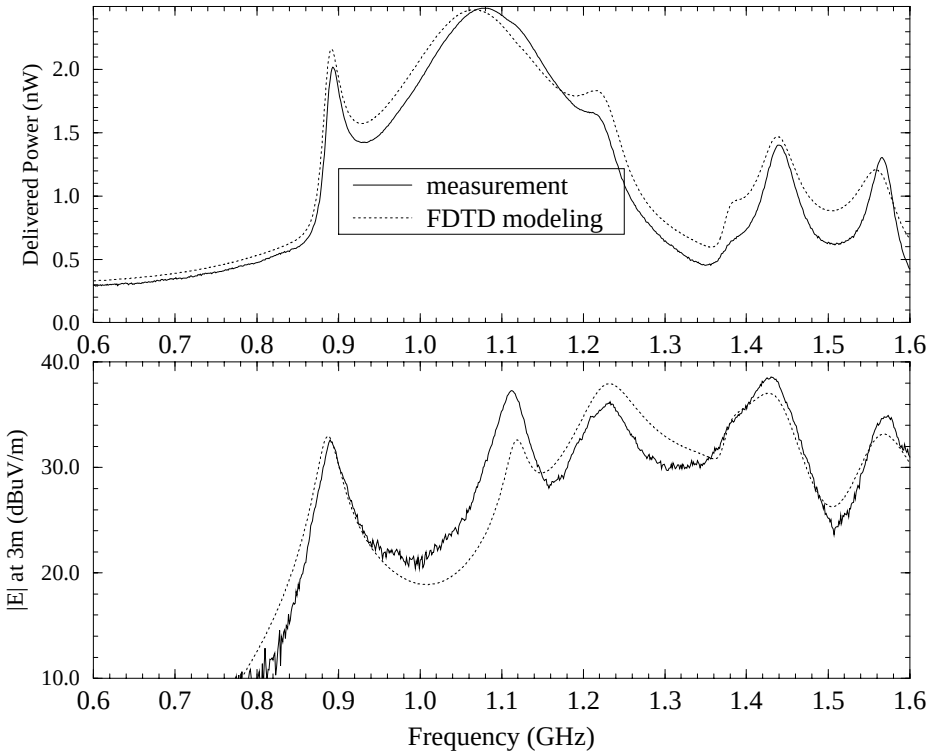

Figure 5. Measured and modeled delivered power and electric field at *3 m* for the test enclosure with a *110Ω /*square lossy material on one wall.

References

[1] D. M. Hockanson, J. L. Drewniak, T. H. Hubing & T. P. Van Doren, "FDTD modeling of common-mode radiation from cables," *IEEE Trans. Electromagn. Compat.,* vol. 38, pp. 376-387, August 1996.

[2] Yuh-Sheng Tsuei, A. C. Cangellaris and J. L. Prince, "Rigorous electromagnetic modeling of chip-to-package (first-level) interconnections," *IEEE Trans. Components Hybrids Manuf. Technol.* vol. 16, pp.876-882, December 1993.

[3] J. Gilbert and R. Holland, "Implementation of the thin-slot formalism in the finite-difference EMP code THREDII," *IEEE Trans. Nucl. Sci.*, vol. NS-28, pp. 4269-4274, December 1981.

[4] M. Li, K-P. Ma, J. L. Drewniak, T. H. Hubing, and T. P. Van Doren, "Numerical and experimental corroboration of an FDTD thin-slot model for slots near corners of shielding enclosures", *IEEE Trans. Electromagn. Compat.,* vol. 39, pp. 225-232, August 1997.

[5] C. A. Balanis, *Advanced Engineering Electromagnetics;* John Wiley & Sons; New York, 1989.

[6] M. Li, J. Nuebel, J. L. Drewniak, R. E. DuBroff, T. H. Hubing, and T. P. Van Doren "EMI from cavity modes of shielding enclosures -- FDTD modeling and measurements", submitted to *IEEE Trans. Electromagn. Compat.*, October 1998.

[7] J. P. Berenger, "Perfectly matched layer for the absorption of electromagnetic waves," *J. Comput. Phys.*, vol. 114, pp. 185-200, October 1994.

[8] D. M. Pozar, *Microwave Engineering;* Addison Wesley; 1990.
[9] D. Morgan, *A Handbook for Testing and Measurement;* Peter Peregrinus Ltd., on behalf of IEE; 1994.
[10] M. Li, S. Radu, J. L. Drewniak, T. H. Hubing, T. P. VanDoren, R. E. DuBroff, *Technical Report TR98-1-029*, Electromagnetic Compatibility Lab., University of Missouri-Rolla.